

Observation of Phonon Anomaly at the Armchair Edge of Single-Layer Graphene in Air

Wenjing Zhang* and Lain-Jong Li*

Research Center for Applied Sciences, Academia Sinica, Taipei, 11529, Taiwan

Graphene is a 2-dimensional plane of carbon atoms arranged in a honeycomb lattice.^{1,2} The electron–phonon interaction in graphene and graphene-like materials, such as carbon nanotubes,^{3–5} carbon nanohorns, and graphene nanoribbons,⁶ has attracted much attention because electrons and phonons exhibit strong coupling in sp^2 -hybridized carbon materials. In the case of single-layer graphene (SLG), the electrons exhibit a linear dispersion near the Fermi energy at the K point in its Brillouin zone. The peculiar band structure of SLG results in the breakdown of the adiabatic (Born–Oppenheimer) approximation,^{7–9} a shift of E_{2g} phonon frequency as a function of charge carrier concentration. The electron–phonon coupling also generates a phonon energy decrease (softening) at Γ and K points, which is known as the Kohn anomaly (KA).^{5,10–12}

The electrical field effect has been used to modulate the charge carrier density in graphene and the KA has been observed in the center area of a graphene sheet, where the Raman spectrum of Γ -point phonon modes (known as the Raman G band) stiffens and sharpens for both electron and hole doping.¹³ The G band stiffening is due to the nonadiabatic removal of KA from the Γ -point, and the G band sharpening is caused by the blockage of the decay channel of phonons into electron–hole pairs. Assuming that graphene is infinite without an edge, the longitudinal and transverse optical phonon (LO and TO) modes are degenerate and contribute equally to the single peak of G band. Sasaki *et al.* have theoretically described that the Raman intensity of the LO and TO modes is asymmetrical at the armchair and zigzag edges, where only the LO (TO) mode is Raman active near the armchair (zigzag) edge.¹⁴ They also predict that the LO mode for both armchair and zigzag edges undergo a strong KA, and their

ABSTRACT Confocal Raman spectroscopy is used to study the phonon modes of mechanically exfoliated single-layer graphene sheets in ambient air. We observe that ambient gas induces obvious shifts in the G band frequency as well as the change in intensity ratio of 2D and G bands, $I(2D)/I(G)$, owing to the Fermi energy change by ambient gas doping. The change in $I(2D)/I(G)$ for the armchair edge is significantly larger than those for the graphene center or zigzag edge in our graphene samples. Also, the G band phonon anomaly, the G band frequency softens and peak width broadens at the charge neutral (Dirac) point, is clearly identified at the armchair edge but not for the zigzag edge or graphene center. We conclude that Fermi level of the armchair edge is close to the Dirac point, making the phonon anomaly visible. However, the charge carrier concentration at the graphene center was too high (Fermi level away from the Dirac point), which completely smears out the phonon softening phenomenon. This study proves that the phonon anomaly can occur at the armchair edge as predicted by Sasaki *et al.* (*J. Phys. Soc. Jpn.* 2010, 79, 044603). Our results also demonstrate that the phonon property of an edge or center site in single-layer graphene is very sensitive to its local carrier concentration.

KEYWORDS: graphene · raman spectroscopy · armchair edge · phonon anomaly · electrical gating · electron–phonon interaction

Raman intensity is enhanced when the polarization of the incident laser is parallel (perpendicular) to the armchair (zigzag) edge.^{14,15} Recently, Cong *et al.* have experimentally observed the polarization dependence of G band intensity at both edges.¹⁶ Nevertheless, the predicted KA phenomenon for the armchair edge is still lacking experimental evidence. Here, we study the Raman features of mechanically exfoliated SLG on SiO_2 substrates in ambient. The graphene was gated through SiO_2 dielectrics using bottom Si-gate. By analyzing the mapping for the intensity ratio of 2D and G bands, $I(2D)/I(G)$, it is observed that our exfoliated SLG was initially *n*-doped. Interestingly the armchair edge was initially closer to the Dirac point compared with the zigzag edge or graphene center. KA phenomenon was clearly identified at the armchair edge but not for the center because the charge carrier concentration at a graphene center is too high (away from the Dirac point), which completely smears out

* Address correspondence to
wjzhangpku@gmail.com,
lanceli@gate.sinica.edu.tw.

Received for review February 10, 2011
and accepted March 9, 2011.

Published online ■ ■ ■
10.1021/nn200550g

© XXXX American Chemical Society

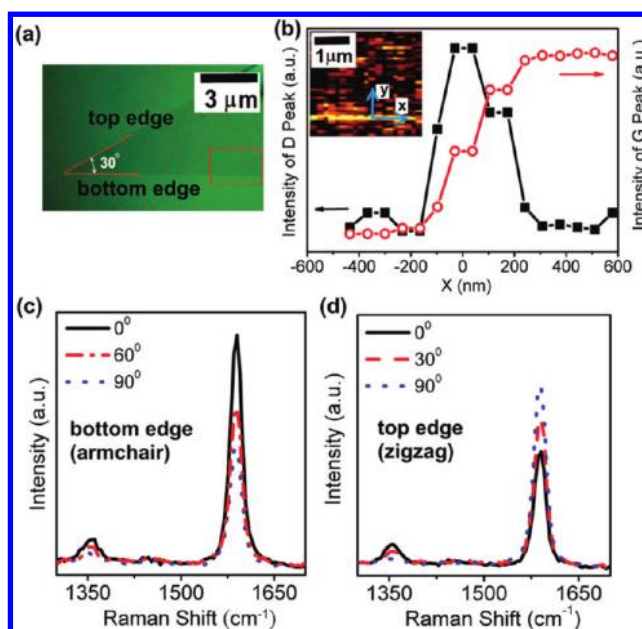


Figure 1. (a) Optical micrograph for a SLG with a 30° angle between two edges. (b) Intensity of G and D bands as a function of position near the bottom edge. Inset shows the Raman mapping of the integrated D band for the SLG. (c) The intensity of G peak for the bottom edge is the strongest when the laser polarization is parallel to it. (d) The intensity of G peak for the top edge is the strongest when the laser polarization is perpendicular to it.

the phonon softening. This study proves that the KA can occur at the armchair edge and the phonon property of an edge or center site in SLG is very sensitive to their local carrier concentration.

RESULTS AND DISCUSSION

The dependence of Raman G band intensity on the laser polarization direction was used to identify the property of graphene edges (armchair- or zigzag-dominated) as reported by Cong *et al.*¹⁶ The SLG sample with a 30° angle shown in Figure 1a is taken as an example to illustrate the procedure. For convenience, we define the direction along the bottom edge as the x-axis and the direction perpendicular to the edge is the y-axis. Inset of Figure 1b displays the Raman mapping of the integrated D band intensity for this sample in the area near the bottom edge indicated as a rectangle in Figure 1a. The D-band (disorder mode; at around 1350 cm^{-1}) is observable only close to the edge, consistent with the literature.^{17–19} Because the laser spot size of confocal Raman spectroscopy is limited by optical diffraction ($\sim 500\text{ nm}$ in our system) it is unlikely to locate the exact edge site. We plot in Figure 1b the peak intensity of D and G bands along the y axis for a selected x-position. We can then define the location of the edge (for a specific x position) at the y-position which exhibits the strongest D-band intensity, where the G band intensity at this point is only half of its full intensity as expected. Also, Figure 1c shows that the intensity of G peak for the bottom edge is the strongest when the polarization orientation of the excitation laser is parallel to the edge, and is the smallest when the polarization orientation is

perpendicular the edge, indicating that the edge is dominated by armchair configurations.^{14–16} By contrast, the polarization dependence of the top edge (Figure 1d) is distinctly different from the bottom edge, and it agrees well with the reported features for a zigzag-dominated edge. It is also noted that the D band intensity at the armchair edge is maximum when the excitation laser polarization is parallel to the edge (Figure 1c), consistent with the theoretical description for the armchair edge.¹⁵ In addition, it is well-known that the Raman selection rule only allows D band Raman-active at the armchair edge but not at the zigzag edge.^{17,18,20,21} Therefore, the presence of D band in Figure 1d and the similar polarization dependence to the armchair-dominated edge (Figure 1c) lead to the conclusion that the zigzag-dominated edge is also composed of some armchair configurations.

Figure 2a shows the G band frequency mapping of the same graphene sample as mentioned in Figure 1. For this sample, the G band frequency of the armchair (bottom) edge is higher than those of the zigzag (top) edge and the graphene center ($>3\text{ cm}^{-1}$). Similar to the observation with the G band, Figure 2b shows that the armchair edge is also with much higher 2D frequency ($>5\text{ cm}^{-1}$) compared with the zigzag edge and graphene center. It has been reported that tensile (compressive) strain can lower (increase) the frequencies of G and 2D band and that the frequency of the 2D band is more sensitive to the strain.²² So the compressive strain might be the reason for the blue shift at the armchair edge. It should be noted that the armchair edge does not necessarily always have a higher G and 2D frequency compared to the graphene center.

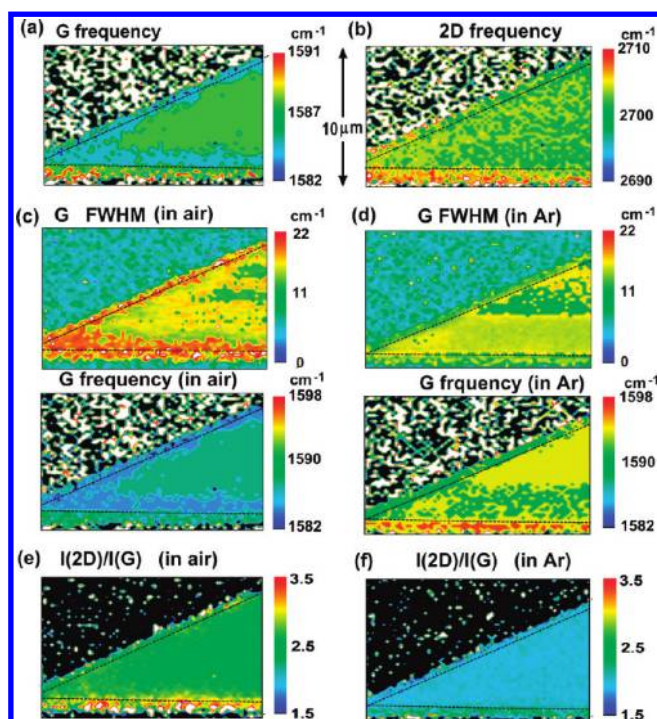


Figure 2. (a) G band frequency and (b) 2D band frequency mappings of the same SLG as discussed in Figure 1a. (c,d) The mappings for the full width at half-maximum (FWHM) and peak frequency of Raman G band obtained (c) in ambient air and (d) in Ar atmosphere. (e,f) The mappings of $I(2D)/I(G)$ obtained (e) in ambient and (f) in Ar atmosphere. The width and height of all mappings are 13 and 10 μm , respectively.

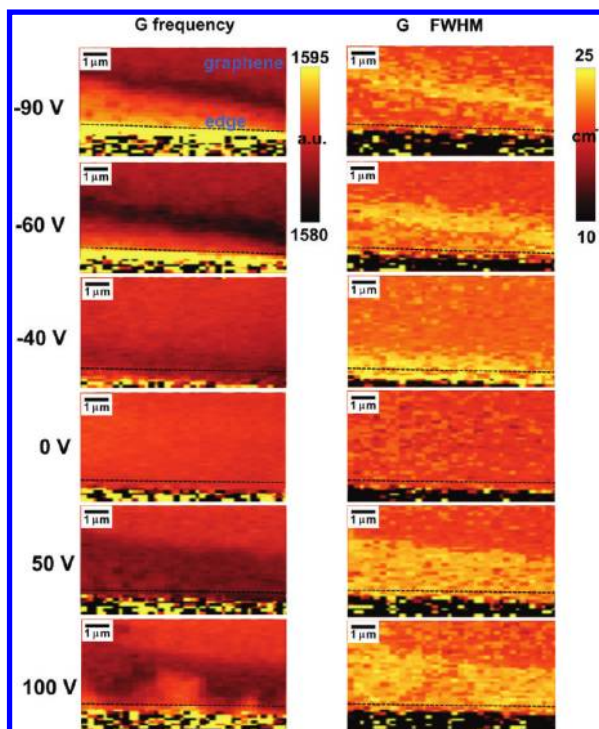


Figure 3. Raman mappings of G band frequency and FWHM at various V_g , where the SLG is grounded on a 300 nm SiO_2 and the V_g is applied to the highly doped-Si underlying SiO_2 .

Another sample demonstrates a case where both arm-chair and zigzag edges have lower G and 2D frequencies compared to the graphene center (Supporting Information, Figure S1a,b). However, the

G and 2D frequencies for an edge are consistent; that is, if the G band frequency is higher (lower), the 2D frequency is also higher (lower) than the graphene center. Experimental results conclude that the higher

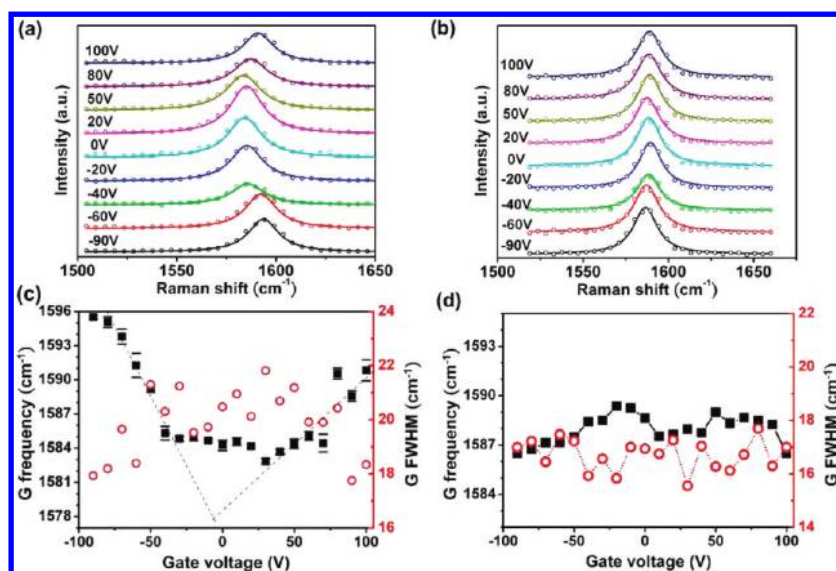


Figure 4. (a) The G band profiles of the armchair edge obtained at various V_g . (b) The G band profiles of the graphene center obtained at various V_g . (c) The G band frequency and FWHM for the armchair edge plotted as a function of V_g . (d) The G band frequency and FWHM for the graphene center plotted as a function of V_g . All spectra and analyses were based on the results in Figure 3.

or lower G and 2D frequencies of the edge are actually sample-dependent. We suspect that the blue- or red-shift of the edges of exfoliated graphene is more likely dominated by the graphene edge uniaxial strain²³ rather than by its intrinsic properties, and the variations in frequency (higher or lower than that of graphene center) may vary with the samples, substrates, and the exfoliation processes.

Figure 2 panels c and d compare the mappings for the full width at half-maximum (FWHM) and peak frequency of Raman G band obtained in ambient and in Ar, respectively (all at room temperature). It is observed that the peak width at the center ranges from 10 to 16 cm^{-1} in Ar and it is slightly broadened to 11–18 cm^{-1} after exposing to the air. Interestingly the peak width for both armchair and zigzag edges significantly increases from the 10–13 in Ar to the 15–22 cm^{-1} in air. We note that the Raman mapping result in air and in Ar is reversible, suggesting that the difference in peak width distribution is caused by the ambient gases such as oxygen and moisture. Many reports have revealed that the ambient oxygen and moisture can *p*-dope the SLG.^{24–27} It has also been revealed that, for intentional doping in graphene using electrochemical or electric gating, G band frequency decreases and peak width increases when the Fermi energy of SLG moves closer to its Dirac point.^{28–30} Figure 2 panels c and d suggest that the Fermi energies of the SLG center and zigzag and armchair edges all move closer to the Dirac point after exposure from Ar to the air environment. It is noted that the changes (G frequency decrease and peak width increase) at the armchair edge seems to be more pronounced compared with those at the graphene center and zigzag edge. Figure 2 panels e and f further reveal that the

intensity ratio $I(2D)/I(G)$ significantly increases upon the exposure to the air. The $I(2D)/I(G)$ has been used to indicate the Fermi level (or doping level) of a SLG, where the value is higher when the Fermi level moves closer to the Dirac point.²⁸ The results in Figure 2 panels e and f confirm that the Fermi level of the center and edges for the SLG shifts toward the Dirac points upon *p*-doping. By taking into account the *p*-doping effect, we conclude that our SLG graphene was initially *n*-doped in Ar and became less *n*-doped after exposure to air. It is noteworthy that the changes in G band frequency and $I(2D)/I(G)$ for the armchair edge are larger than those for the center and zigzag edge, indicating that the Fermi level of the armchair edge is closer to the Dirac point compared with the graphene center and the zigzag edge.

To further elucidate the phonon properties of the armchair edge in air, we systematically study the gate voltage (V_g) dependence of its Raman spectra. Figure 3 shows the Raman mappings of G band frequency and FWHM at various V_g , where the SLG is grounded on a 300 nm SiO_2 and the V_g is applied to the highly doped Si underlying SiO_2 to generate electrical field for tuning the Fermi energy of the SLG. The evolution of Raman mappings as a function of V_g demonstrates that the electric field results in significant changes in the frequency and lifetime of phonons at the armchair edge, but the center area exhibits relatively unpronounced changes. The results in Figure 3 were summarized and discussed in Figure 4. Figure 4a displays the G band profiles of the armchair edge obtained at various V_g , while those for the center area were displayed in Figure 4b. It is noted that each Raman spectrum shown in Figure 4a (4b) was obtained after averaging 10 spectra selected from different sites

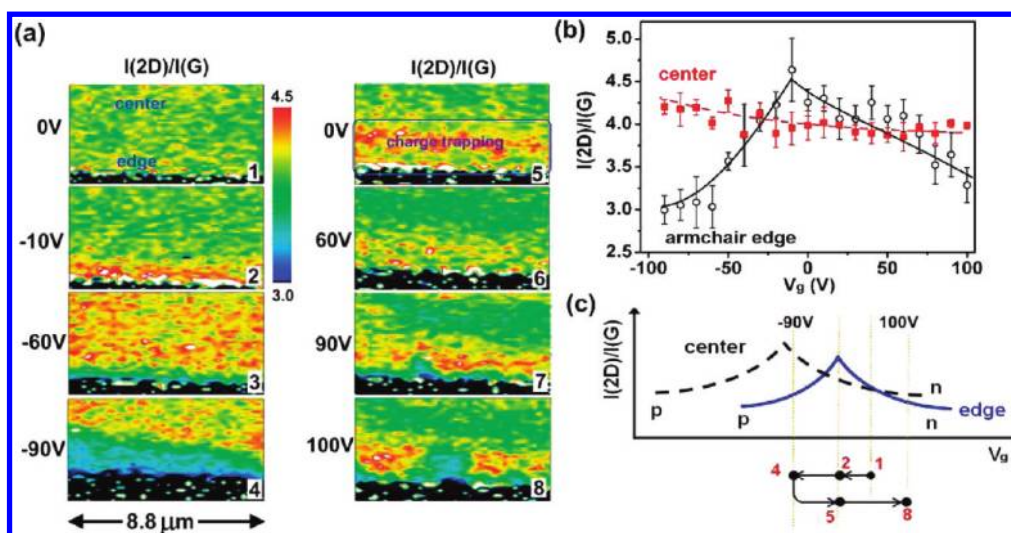


Figure 5. (a) The mappings of $I(2D)/I(G)$ for the area taken near the armchair edge at several selected V_g . The mappings were derived from the results obtained for the sample as in Figure 3. (b) The extracted $I(2D)/I(G)$ values at the armchair edge and the center. (c) Schematic illustration for the gate voltage dependence on the $I(2D)/I(G)$ profile for the armchair edge and graphene center. The tuning range of the Fermi level in our experiment (between -90 and 100 V) is also indicated. The width and height of all mappings in panel a are 8.8 and $4.4 \mu\text{m}$, respectively.

of the armchair edge (center). The gate voltage dependences for the spectra in Figure 4 panels a and b were shown in Figure 4 panels c and d, respectively. For the armchair edge, the increase in charge density of either electron or hole results in the G band stiffening. The FWHM of G band decreases as the applied V_g is large enough, showing that longer phonon lifetime is linked to higher electron or hole density, which is the typical phenomena of KA. The result in Figure 4c shows that application of $V_g = 100$ V produced a 10 cm^{-1} G band shift to higher energy, which is consistent with several recent reports on KA of bulk graphene.^{29–31} The G band FWHM of our armchair edge is significantly broader than that reported in ref 29, even at higher gate voltages, which is likely attributed to several effects: (i) The broadening caused by ambient gases (increase by $5–9 \text{ cm}^{-1}$) as discussed in Figure 2. (ii) The broadening caused by ambient temperature. Yan *et al.* have reported that a G band tail can develop at the low energy side in a low carrier density regime,³² which may contribute to the broadening. (iii) The broadening caused by defects at the edge. Ferreira *et al.* have shown that the G band peak width increases with the defect (or disorder) density.³³ We believe that the unavoidable structure disorder at graphene edges as well as the effect from ambient gases significantly increases the G band width in our measurements. It is also observed in Figure 4c that the G frequency is asymmetric (the change for positive V_g is smaller than negative V_g), which is consistent with the prediction based on Born–Oppenheimer approximation that the adiabatic contribution can result in the electron–hole asymmetry.¹³ However, it is still not possible to exclude the contribution from the trapped electrons in SiO_2 , which screen off part of the gate field under

positive V_g and contribute to the asymmetric behaviors.⁵ The two regressed lines for the G frequency data points at high carrier density (corresponding to large negative and positive V_g) intercepts at a negative V_g (around -10 V), suggesting the armchair edge is *n*-doped in ambient when V_g is 0. The G frequency for the SLG center does not exhibit obvious dependence on V_g , likely because the SLG contains large amounts of charge impurities, which will be further discussed in Figure 5. We note that the G band frequency and FWHM of the zigzag edge is also insensitive to the change of applied V_g (see Supporting Information, Figure S2). The origin of the insensitivity for the zigzag edge is due to the Raman selection rule,^{14,15} where the LO phonon modes (KA-related) are Raman inactive for zigzag edges.

To study the origin of the distinct behavior of the armchair edge, we plot in Figure 5a the mappings of $I(2D)/I(G)$ at several selected V_g , where the Raman measurements were following the sequence $V_g = 0$ V, -10 V, -20 V, ..., -90 V, 0 V, 10 V, 20 V, ..., and 100 V. The $I(2D)/I(G)$ ratio at the center is less sensitive to the V_g ; the only observable change is the slight increase when the gate is applied with large negative V_g . By contrast, the $I(2D)/I(G)$ for the armchair edge significantly decreases upon increasing the charge carrier density with both positive and negative V_g . Figure 5b summarizes the extracted $I(2D)/I(G)$ values at the armchair edge and the center. It is concluded that armchair is much more sensitive to the SLG center and the Dirac point of the armchair edge can be easily identified at around -10 V, agreeing with our conclusions drawn from Figure 4. The previous discussions for Figure 2 have already indicated that armchair is more sensitive to the doping from the environment. As indicated as point 1

in Figure 5c, the armchair edge is initially at the electron-rich regime (n -doped) and close to the Dirac point. With the application of a negative V_g , the Fermi level shifts across the Dirac point at -10 V. Further increase in negative V_g results in a lower $I(2D)/I(G)$ value (point 4 in Figure 5c). It is noted that the $I(2D)/I(G)$ value in some areas of mapping 5 (Figure 5a at $V_g = 0$) still remain high after the removal of negative voltages, and does not fully recover to its initial situation (mapping 1 of Figure 5a; $V_g = 0$) due to the electron trapping in SiO_2 . The trapping effect is obviously seen in the area closer to the edge (width $\approx 1.5 \mu\text{m}$ from the edge to the interior as indicated in mapping 5). Because the Fermi energy for the area closer to the edge is near the Dirac point at $V_g \approx 0$, small amounts of charge trapping are likely to cause obvious change in $I(2D)/I(G)$. When positive V_g is applied to the sample, the Fermi level for the armchair edge shifts back to the n -doped regime and the $I(2D)/I(G)$ value is lowered. The trapped electrons in SiO_2 effectively reduce the electrical field provided to the armchair edge and result in smaller change on the right-hand branch of $I(2D)/I(G)$ curve in Figure 5b. On the basis of the mapping results, we conclude that the SLG center area is far away from the Dirac point. It is believed that the unintentional n -doping from charge impurities effectively screens off the applied electrical field; hence, the $I(2D)/I(G)$ profile is left-shifted as schematically illustrated in Figure 5c, resulting in the insensitivity of

the phonon anomaly to the applied gate voltage. Note that the charge impurities on the SiO_2 substrates have been found to effectively dope the graphene layer on top.³⁴ The impurities introduced during the mechanical exfoliation such as tape adhesives may also contribute to the unintentional doping.

CONCLUSIONS

We have shown that the p -doping caused by the ambient gas shifts the Fermi energy of the armchair edge to a level very close to the Dirac point, which makes the phonon anomaly visible at the armchair edge but not for the zigzag edge or graphene center. The charge carrier concentration at graphene center was too high (Fermi level away from the Dirac point), which completely smears out the phonon softening phenomenon. Our results demonstrate that phonon property of the edge or center site in graphene is governed by the local carrier concentration (or Fermi level alignment to the Dirac point). It is still unclear why the Fermi energy of the armchair edge is closer to the Dirac point. Although the energy of the pure armchair edge has been predicted to be lower than the zigzag edge,²³ the zigzag edge may become even more stable than the armchair edge by edge reconstruction.³⁵ More investigations are required to reveal whether the intrinsic electronic structure or the physisorption/chemisorption reactivity dominates the Fermi energy of different edges.

EXPERIMENTAL SECTION

Raman Measurements. Raman spectra were collected using a WITec CRM300 confocal Raman microscopy system (with a laser wavelength of 488 nm and laser spot size of $\sim 0.5 \mu\text{m}$), and the Si peak at 520 cm^{-1} was used as a reference for wavenumber calibration. For the Raman results in Figure 2 (comparison in Ar and in air), the NT-MDT confocal Raman system with airtight enclosure was used (a laser wavelength of 473 nm and laser spot size of $\sim 0.5 \mu\text{m}$).

Acknowledgment. This research was mainly supported by Research Center for Applied Science, Academia Sinica (Nano program), and National Science Council Taiwan (NSC-99-2112-M-001-021-MY3 and 99-2738-M-001-001). We are also grateful for the support from Singapore CRP program: NRF-CRP2-2007-02.

Supporting Information Available: Supporting Raman spectra and mappings. This material is available free of charge via the Internet at <http://pubs.acs.org>.

REFERENCES AND NOTES

- Novoselov, K. S.; Geim, A. K.; Morozov, S. V.; Jiang, D.; Zhang, Y.; Dubonos, S. V.; Grigorieva, I. V.; Firsov, A. A. Electric Field Effect in Atomically Thin Carbon Films. *Science* **2004**, *306*, 666–669.
- Geim, A. K.; Novoselov, K. S. The Rise of Graphene. *Nat. Mater.* **2007**, *6*, 183–191.
- Maciel, I. O.; Anderson, N.; Pimenta, M. A.; Hartschuh, A.; Qian, H.; Terrones, M.; Terrones, H.; Campos-D., J.; Rao, A. M.; Novotny, L.; *et al.* Electron and Phonon Renormalization Near Charged Defects in Carbon Nanotubes. *Nat. Mater.* **2008**, *7*, 878–883.
- Farhat, H.; Son, H.; Samsonidze, G. G.; Reich, S.; Dresselhaus, M. S.; Kong, J. Phonon Softening in Individual Metallic Carbon Nanotubes Due to The Kohn Anomaly. *Phys. Rev. Lett.* **2007**, *99*, 145506.
- Tsang, J. C.; Freitag, M.; Perebeinos, V.; Liu, J.; Avouris, Ph. Doping and Phonon Renormalization in Carbon Nanotubes. *Nat. Nanotechnol.* **2007**, *2*, 725–730.
- Sasaki, K.; Yamamoto, M.; Murakami, S.; Saito, R.; Dresselhaus, M. S.; Takai, K.; Mori, T.; Enoki, T.; Wakabayashi, K. Kohn Anomalies in Graphene Nanoribbons. *Phys. Rev. B* **2009**, *80*, 155450-1–155450-11.
- Pisana, S.; Lazzeri, M.; Casiraghi, C.; Novoselov, K. S.; Geim, A. K.; Ferrari, A. C.; Mauri, F. Breakdown of the Adiabatic Born–Oppenheimer Approximation in Graphene. *Nat. Mater.* **2007**, *6*, 198–201.
- Stampfer, C.; Molitor, F.; Graf, D.; Ensslin, K.; Jungen, A.; Hierold, C.; Wirtz, L. Raman Imaging of Doping Domains in Graphene on SiO_2 . *Appl. Phys. Lett.* **2007**, *91*, 241907.
- Yan, J.; Zhang, Y.; Goler, S.; Kim, P.; Pinczuk, A. Raman Scattering and Tunable Electron-Phonon Coupling in Single Layer Graphene. *Solid State Commun.* **2007**, *143*, 39–43.
- Kohn, W. Image of the Fermi Surface in the Vibration Spectrum of a Metal. *Phys. Rev. Lett.* **1959**, *2*, 393–394.

- Ando, T. Anomaly of Optical Phonon in Monolayer Graphene. *J. Phys. Soc. Jpn.* **2006**, *75*, 124701.
- Piscanec, S.; Lazzeri, M.; Mauri, F.; Ferrari, A. C.; Robertson, J. Kohn Anomalies and Electron-Phonon Interactions in Graphite. *Phys. Rev. Lett.* **2004**, *93*, 185503.
- Lazzeri, M.; Mauri, F. Nonadiabatic Kohn Anomaly in a Doped Graphene Monolayer. *Phys. Rev. Lett.* **2006**, *97*, 266407.
- Sasaki, K.; Saito, R.; Wakabayashi, K.; Enoki, T. Identifying the Orientation of Edge of Graphene Using G Band Raman Spectra. *J. Phys. Soc. Jpn.* **2010**, *79*, 044603–1–044603–8.
- Sasaki, K.-I.; Wakabayashi, K.; Enoki, T. Polarization Dependence of Raman Spectra in Strained Graphene. *Phys. Rev. B.* **2010**, *82*, 205407.
- Cong, C.; Yu, T.; Wang, H. Raman Study on The G Mode of Graphene for Determination of Edge Orientation. *ACS Nano* **2010**, *4*, 3175–3180.
- Cancado, L. G.; Pimenta, M. A.; Neves, B. R. A.; Dantas, M. S. S.; Jorio, A. Influence of the Atomic Structure of The Raman Spectra of Graphite Edges. *Phys. Rev. Lett.* **2004**, *93*, 247401.
- You, Y. M.; Ni, Z. H.; Yu, T.; Shen, Z. X. Edge Chirality Determination of Graphene by Raman Spectroscopy. *Appl. Phys. Lett.* **2008**, *93*, 163112–1–163112–3.
- Casiraghi, C.; Hartschuh, A.; Qian, H.; Piscanec, S.; Georgi, C.; Fasoli, A.; Novoselov, K. S.; Basko, D. M.; Ferrari, A. C. Raman Spectroscopy of Graphene Edges. *Nano Lett.* **2009**, *9*, 1433–1441.
- Malard, L.; Pimenta, M.; Dresselhaus, G.; Dresselhaus, M. Raman spectroscopy in graphene. *Phys. Rep.* **2009**, *473*, 51–87.
- Gupta, A. K.; Russin, T. J.; Gutierrez, H. R.; Eklund, P. C. Probing Graphene Edges via Raman Scattering. *ACS Nano* **2009**, *3*, 45–52.
- Tsoukleri, G.; Parthenios, J.; Papagelis, K.; Jalil, R.; Ferrari, A. C.; Geim, A. K.; Novoselov, K. S.; Galotis, C. Subjecting a Graphene Monolayer to Tension and Compression. *Small* **2009**, *5*, 2397–2402.
- Huang, B.; Liu, M.; Su, N.; Wu, J.; Duan, W.; Gu, B.-L.; Liu, F. Quantum Manifestations of Graphene Edge Stress and Edge Instability: A First-Principles Study. *Phys. Rev. Lett.* **2009**, *102*, 166409.
- Liu, L.; Ryu, S.; Tomasik, M. R.; Stolyarova, E.; Jung, N.; Hybertsen, M. S.; Steigerwald, M. L.; Brus, L. E.; Flynn, G. W. Graphene Oxidation: Thickness-Dependent Etching and Strong Chemical Doping. *Nano Lett.* **2008**, *8*, 1965–1970.
- Giannozzi, P.; Car, R.; Scoles, G. Oxygen Adsorption of Graphite and Nanotubes. *J. Chem. Phys.* **2003**, *118*, 1003–1006.
- Schedin, F.; Geim, A. K.; Morozov, S. V.; Hill, E. W.; Blake, P.; Katsnelson, M. I.; Novoselov, K. S. Detection of Individual Gas Molecules Adsorbed on Graphene. *Nat. Mater.* **2007**, *6*, 652–655.
- Shi, Y.; Fang, W.; Zhang, K.; Zhang, W.; Li, L. J. Photoelectrical Response in Single-Layer Graphene Transistors. *Small* **2009**, *5*, 2005–2011.
- Das, A.; Pisana, S.; Chakraborty, B.; Piscanec, S.; Saha, S. K.; Waghmare, U. V.; Novoselov, K. S.; Krishnamurthy, H. R.; Geim, A. K.; Ferrari, A. C.; *et al.* Monitoring Dopants by Raman Scattering in an Electrochemically Top-Gated Graphene Transistor. *Nat. Nanotechnol.* **2008**, *3*, 210–215.
- Yan, J.; Zhang, Y.; Kim, P.; Pinczuk, A. Electric Field Effect Tuning of Electron-Phonon Coupling in Graphene. *Phys. Rev. Lett.* **2007**, *98*, 166802.
- Zhou, S. Y.; Siegel, D. A.; Fedorov, A. V.; Lanzara, A. Kohn Anomaly and Interplay of Electron–Electron and Electron–Phonon Interactions in Exfoliated Graphene. *Phys. Rev. B* **2008**, *78*, 193404.
- Casiraghi, C.; Pisana, S.; Novoselov, K. S.; Geim, A. K.; Ferrari, A. C. Raman Fingerprint of Charged Impurities in Graphene. *Appl. Phys. Lett.* **2007**, *91*, 233108.
- Yan, J.; Zhang, Y.; Goler, S.; Kim, P.; Pinczuk, A. Raman Scattering and Tunable Electron–Phonon Coupling in Single Layer Graphene. *Solid State Commun.* **2007**, *143*, 39–43.
- Ferreira, E. H.; Moutinho, M. V. O.; Stavale, F.; Lucchese, M. M.; Capaz, R. B.; Achete, C. A.; Jorio, A. Evolution of the Raman Spectra from Single-, Few-, and Many-Layer Graphene with Increasing Disorder. *Phys. Rev. B* **2010**, *82*, 125429.
- Shi, Y.; Dong, X.; Chen, P.; Wang, J.; Li, L. J. Effective Doping of Single-Layer Graphene from Underlying SiO₂ Substrates. *Phys. Rev. B* **2009**, *79*, 115402.
- Koskinen, P.; Malola, S.; Hakkinen, H. Self-Passivating Edge Reconstructions of Graphene. *Phys. Rev. Lett.* **2008**, *101*, 115502.